SCIPEDIA

Boundary Element Analysis of a Semi-Infinite Anisotropic Plane Containing Inclusions/Holes

Yui-Chuin Shiah* and Chao-Chun Ko

Department of Aeronautics and Astronautics, National Cheng Kung University, Tainan, 701, Taiwan

INFORMATION

Keywords:
Boundary element method
anisotropic elasticity
semi-infinite plane
inclusions/holes

DOI: 10.23967/j.rimni.2025.10.59576

SCIPEDIA Revista Internacional de Métodos Numéricos para Cálculo y Diseño en Ingeniería

RIMNI Revista Internacional Métodos numéricos para cálculo y diseño en ingeniería

Boundary Element Analysis of a Semi-Infinite Anisotropic Plane Containing Inclusions/Holes

Yui-Chuin Shiah* **and Chao-Chun Ko**

Department of Aeronautics and Astronautics, National Cheng Kung University, Tainan, 701, Taiwan

ABSTRACT

In this article, the fundamental solutions with Lekhnitskii-like formulations are implemented in the boundary element method (BEM) to calculate the Two-dimensional elastostatic field in a semi-infinite anisotropic plane containing inclusions/holes. In addition to the source point in the semi-infinite plane, four pseudo-sources are superposed to provide traction-free conditions on the plane surface. To avoid mesh modeling at infinity, the fundamental solutions are modified so that the displacements/stresses at the far field automatically vanish. For modeling problems in civil engineering, loading on the plane surface can be specified as part of the boundary condition. When embedded holes are present in the half-plane, loading on the holes can also be applied. Using the sub-region technique, the elastic field in the half-plane containing inclusions can also be investigated. Studies of a few examples indicate that the proposed BEM is a very efficient and versatile methodology to investigate many practical problems, especially in civil engineering.

OPEN ACCESS

Received: 11/10/2024

Accepted: 10/01/2025

Published: 07/04/2025

DOI
10.23967/j.rimni.2025.10.59576

Keywords:
Boundary element method
anisotropic elasticity
semi-infinite plane
inclusions/holes

1 Introduction

This article aims to investigate the elastic field of an anisotropic half-plane containing inclusion(s)/hole(s) as schematically depicted in Fig. 1. Such applications in practice can be commonly seen in material sciences (e.g., [1,2]) and geomechanics (e.g., [3,4]). In the past, various studies of these problems have applied either analytical approaches or numerical simulations. Due to mathematical complexities, analytical approaches are only successful for simple cases with regular geometries like circular or elliptical inclusions/holes (e.g., [5,6]). The finite element method (FEM) has been applied to study the interaction among multiple nanocavities (e.g., [7,8]); however, very fine meshes are required for the FEM to ensure accurate solutions.

More examples of the FEM studying half-plane problems can be found in [9–11] for example. Despite its generality in treating various issues, the FEM is not a good choice for modeling unbounded domains like an infinite/semi-infinite plane. As powerful alternatives, other numerical methods include the boundary element method (BEM), the local integration equation method (e.g., [12]), and the radial basis function method (e.g., [13]). For studying the problem of inclusions, a combination of the

*Correspondence: Yui-Chuin Shiah (ycshiah@mail.ncku.edu.tw).

boundary element method and the radial basis function method was applied [14]. Using the boundary point method as an addition to the examples, Dong et al. [15] performed stress analysis of an infinite anisotropic elastic medium with elastic inclusions. Not falling within the present scope of this article, no further discussions about other numerical approaches are intended here.

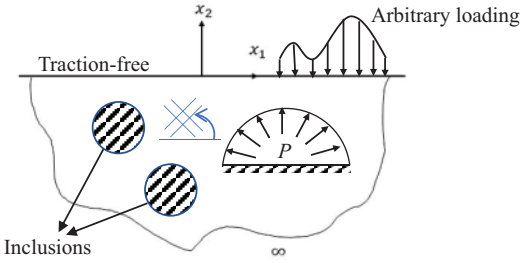

Figure 1: Anisotropic half-plane containing inclusion(s)/hole(s)

As a major advantage of the BEM, only boundary discretization is needed but not for the entire domain. This advantage is even more obvious in modeling problems of infinite/semi-infinite planes containing inclusions/holes when the conventional domain solution techniques encounter difficulties in modeling unbounded domains and irregular geometry of the inclusions/holes. For this advantage, this article targets studying the stress field in an anisotropic half-plane (sometimes also referred to as a semi-infinite plane) containing inclusions/holes. In the past, pertinent BEM works reported in the literature mostly considered isotropic media. To name a few examples, Green's functions of isotropic half-planes were derived in [16,17] and implemented in their BEM analyses. Dong et al. [18] carried out stress analyses of elastic isotropic half-plane containing nano inhomogeneities with surface/interface effects. Using the complex variables boundary element method, more related works of treating isotropic half-planes can also be found in [19]. The boundary integral equation (BIE) and the associated Green's function for orthotropic half-plane problems were given in [20]. Related works for treating infinite/semi-infinite anisotropic planes have remained relatively much less. Using Lekhnitskii's fundamental solutions [21], Tan et al. [22] employed the BEM to study the stress field near inclusions in an infinite anisotropic matrix, where comparably large side-length of a finite domain was taken to model infinite boundaries.

By following the one-complex function method introduced by Suo [23], Pan et al. [24] first presented Green's functions for anisotropic half-planes, by which the particular solutions of gravity and far-field stresses were also derived in the work as well [25–27]. More recent works regarding the half-plane problem can be referred to [28–32]. In the present work, Stroh's formalism [33] is followed to give the explicit expressions of Lekhnitskii-like fundamental solutions for anisotropic half-planes, by which the traction-free conditions on the half-plane surface are automatically satisfied. For obtaining Green's functions of anisotropic half-planes, the fundamental solutions are further modified for the corresponding displacements and stresses to vanish at far fields. All formulations are implemented in an existing BEM code for studying the stresses on inclusions/holes in an anisotropic half-plane, where arbitrary loading can also be prescribed on the plane surface as an option. A few numerical examples are presented at the end for illustration of the successful implementation.

2 Boundary Integral Equation for 2D Anisotropic Elasticity

As has been well documented in the literature, the BIE to correlate the displacements, denoted by u_j, and the tractions, denoted by t_j, between the source point P and the field point Q over the surface S is expressed as

$$C_{ij}(P)u_i(P) = \int_S U^*_{ij}(P,Q)t_i(Q)\,dS - \int_S T^*_{ij}(P,Q)u_i(Q)dS, \tag{1}$$

where C_{ij} is the free terms for the source point positioned on the boundary. By use of the relation of free body motion (i.e., letting $u_i = 1$, $t_i = 0$ everywhere). In Eq. (1), U^*_{ij} and T^*_{ij} represent respectively the fundamental solution of displacements and tractions in the x_i-direction at Q due to a concentrated load applied in the x_j-direction at P in an infinite elastic body. For completeness, the formulations presented by Lekhnitskii [21] are first outlined. In an infinite anisotropic plane, U^*_{ij} is given by

$$U^*_{ij} = 2\mathbf{Re}\left\{\sum\nolimits_{k=1}^{2} B_{ik}A_{jk}\ln\left(z_k - z'_k\right)\right\}, \tag{2}$$

where A_{jp}, B_{ip} are the material's constants to be described later; z_p and z'_p are defined in terms of the field coordinates at (x_1, x_2) and source coordinates at (x^p_1, x^p_2) by

$$z_k = x_1 + \mu_k x_2,\ \ z'_k = x^p_1 + \mu_k x^p_2. \tag{3}$$

Eq. (2), $\mathbf{Re}\{.\}$ denotes taking the real part of the complex variable inside the curly bracket, and $\mu_k = (\alpha_k + \mathbf{i}\beta_k)$, the material's eigenvalues, are determined from the conjugate roots to the following characteristic equation,

$$a_{11}\mu^4 - a_{16}\mu^3 + (2a_{12} + a_{66})\,\mu^2 - a_{26}\mu + a_{22} = 0, \tag{4}$$

where a_{ij} is the material's compliance coefficients. Following the usual notations of anisotropic mechanical properties, one may determine a_{ij} in terms of the mechanical properties by

$$\begin{aligned} &a_{11} = 1/E_1,\ a_{12} = -\nu_{12}/E_1 = -\nu_{21}/E_2,\ a_{16} = \eta_{12,1}/E_1 = \eta_{1,12}/G_{12},\\ &a_{22} = 1/E_2,\ a_{26} = \eta_{12,2}/E_2 = \eta_{2,12}/G_{12},\ a_{66} = 1/G_{12}. \end{aligned} \tag{5}$$

All the definitions in Eq. (5) are for the state of plane stress. For plane strain, the compliance is replaced by $\hat{a}_{jk}$, redefined by

$$\hat{a}_{jk} = a_{jk} - a_{j3}a_{k3}/a_{33},\ \ (j,k = 1,2,6), \tag{6}$$

where a_{j3} are given by

$$a_{j3} = -\nu_{j3}/E_j = -\nu_{3j}/E_3, \quad a_{33} = 1/E_3, \quad a_{63} = \eta_{12,3}/E_3 = \eta_{3,12}/G_{12}. \tag{7}$$

In Eq. (2), the coefficients B_{ip} and A_{jp} are given by

$$\mathbf{B} = \begin{pmatrix} a_{11}\mu_1^2 - a_{16}\mu_1 + a_{12} & a_{11}\mu_2^2 - a_{16}\mu_2 + a_{12} \\ a_{12}\mu_1 - a_{26} + a_{22}/\mu_1 & a_{22}\mu_2 - a_{26} + a_{22}/\mu_2 \end{pmatrix}, \tag{8}$$

$$\begin{bmatrix} \mathbf{Re}\{\mathrm{A}_{j1}\} \\ \mathbf{Im}\{\mathrm{A}_{j1}\} \\ \mathbf{Re}\{\mathrm{A}_{j2}\} \\ \mathbf{Im}\{\mathrm{A}_{j2}\} \end{bmatrix} = \begin{bmatrix} 0 & 1 & 0 & 1 \\ \beta_1 & \alpha_1 & \beta_2 & \alpha_2 \\ \mathbf{Im}\{\mathrm{B}_{11}\} & \mathbf{Re}\{\mathrm{B}_{11}\} & \mathbf{Im}\{\mathrm{B}_{12}\} & \mathbf{Re}\{\mathrm{B}_{12}\} \\ \mathbf{Im}\{\mathrm{B}_{21}\} & \mathbf{Re}\{\mathrm{B}_{21}\} & \mathbf{Im}\{\mathrm{B}_{22}\} & \mathbf{Re}\{\mathrm{B}_{22}\} \end{bmatrix}^{-1} \begin{bmatrix} -\delta_{j2}/4\pi \\ \delta_{j1}/4\pi \\ 0 \\ 0 \end{bmatrix}, \tag{9}$$

where **Im**{.} is to take the imaginary part of the complex variable inside the curly bracket. Observing Eq. (2), one may notice the fundamental displacements will approach infinity when Q is placed at a far place away from P. For the analysis of inclusions/holes in an infinite plane, the fundamental solution of displacements in Eq. (2) must vanish at infinity such that no discretization is needed at far places. For this purpose, the fundamental displacements, denoted here by $U_{ij}^*\big|_\infty$, are modified to be

$$U_{ij}^*\big|_\infty = \frac{2}{R_\infty}\mathbf{Re}\left\{\sum_{k=1}^{2} B_{ik}A_{jk}\mathbf{ln}\left(\frac{z_k - z_k'}{R_\infty}\right)\right\}, \tag{10}$$

where R_∞ is given a relatively very large value in comparison with the size of the inclusions/holes to be analyzed. The fact, the factor R_∞ is simply a factor associated with rigid body motion, forcing the solutions to vanish at infinity. The corresponding solutions of tractions, denoted hereby $T_{ij}^*\big|_\infty$, are now given by

$$T_{ij}^*\big|_\infty = \frac{2}{R_\infty}\mathbf{Re}\left\{\sum_{k=1}^{2} A_{jk}\hat{\mu}_{ik}\left(\frac{n_1\mu_k - n_2}{z_k - z_k'}\right)\right\}, \tag{11}$$

where $\hat{\mu}_{ik}$ is given by

$$\hat{\mu}_{ik} = \begin{pmatrix} \mu_1 & \mu_2 \\ -1 & -1 \end{pmatrix}. \tag{12}$$

The tractions given above will approach null at infinity as well. Because all solutions in Eqs. (10)–(12) automatically vanish at infinity, one may apply the BIE in Eq. (1) to analyze the stresses in an infinite plane containing holes, yet no discretization is needed to model infinity. Thus, the formulations can be taken as Green's functions to analyze the problems with holes in an infinite anisotropic plane.

3 Green's Functions for Anisotropic Half-Plane

As provided in details using the Stroh's formulism [26], the fundamental solutions for anisotropic half-plane are

$$\boldsymbol{U} = \mathbf{2Re}\{\boldsymbol{A}\,\mathbf{f}\}, \tag{13}$$

$$\begin{bmatrix}\sigma_{11}\\ \sigma_{21}\end{bmatrix} = -\mathbf{Im}\{\mathbf{B} < \mu_\alpha > \mathbf{f}'\}, \quad \begin{bmatrix}\sigma_{12}\\ \sigma_{22}\end{bmatrix} = \mathbf{Im}\{\mathbf{B}\mathbf{f}'\}, \tag{14}$$

where

$$\mathrm{f} = \frac{p}{\pi}\left\{< \mathbf{ln}(Z_\alpha - Z_\alpha') > A^T + \sum_{q=1}^{2} < \mathbf{ln}(Z_\alpha - \overline{Z}_q') > B^{-1}\overline{B}I_q\overline{A}^T\right\}, \tag{15}$$

$$\mathrm{f}' = \frac{P}{\pi}\left\{< \frac{1}{Z_\alpha - Z_\alpha'} > A^T + \sum_{q=1}^{2} < \frac{1}{Z_\alpha - \overline{Z}_q'} > B^{-1}\overline{B}I_q\overline{A}^T\right\}. \tag{16}$$

Detailed definitions of all tensors can be referred to [26]. By simplifying all tensors and making algebraic arrangements, positions of pseudo-sources in the imaged half-plane can be described by two parameters, namely $\hat{z}_{mn}$, defined by

$$\hat{z}_{mn} = z_m - \overline{z}_n', \quad (m, n = 1, 2). \tag{17}$$

As is clear from Eq. (17), the positions of the four additional pseudo-sources for ($m = 1, 2$ and $n = 1, 2$) are completely dependent on the material's properties. With the superposition of the four additional pseudo-sources, Green's function of displacements for an anisotropic half-plane is given by

$$U_{ij}^*\Big|_{\infty/2} = U_{ij}^*\Big|_{\infty} - \frac{2}{R_\infty}\mathbf{Re}\left\{\sum_{m=1}^{2}\sum_{n=1}^{2} B_{im}\overline{A}_{jn}D_{mn}\mathbf{ln}\left(\frac{\hat{z}_{mn}}{R_\infty}\right)\right\}, \tag{18}$$

where D_{mn} is defined by

$$D_{1n} = \frac{-\overline{\mu}_n + \mu_2}{-\mu_1 + \mu_2},\ D_{2n} = \frac{\overline{\mu}_n - \mu_1}{-\mu_1 + \mu_2}. \tag{19}$$

Eq. (18), $U_{ij}^*\Big|_{\infty}$ corresponds to the solutions for an infinite anisotropic plane as given in Eq. (10). Simply for the similarity, Eq. (10) can be considered as a Lekhnitskii-like Green's function for an anisotropic half-plane. By similar procedures, the solutions of tractions for anisotropic half-plane, denoted by $T_{ij}^*\Big|_{\infty/2}$, are written as

$$T_{ij}^*\Big|_{\infty/2} = T_{ij}^*\Big|_{\infty} - \frac{2}{R_\infty}\mathbf{Re}\left\{\sum_{m=1}^{2}\sum_{n=1}^{2} \hat{\mu}_{im}\frac{(n_1\mu_m - n_2)\,\overline{A}_{jn}D_{mn}}{\hat{z}_{mn}}\right\}. \tag{20}$$

The second terms in Eqs. (18) and (20) are contributions of the four additional pseudo-sources to counteract the tractions on the plane produced by the source. In addition to the condition of free tractions on the half-plane surface, null displacements, and tractions will also be satisfied at infinity. Thus, Eqs. (18)–(20) are considered Green's functions for modeling holes in an anisotropic half-plane.

To apply the BIE to analyze the problems of half-plane containing inclusions, considerations are given to two separate cases, that is rigid inclusions or elastic inclusions. For modeling rigid inclusions, one may simply constrain the hole surfaces in all directions. By solving the BIE, tractions on the hole surfaces can thus be determined and further applied on the inclusion surfaces to analyze stresses on the inclusions. For treating elastic inclusions, the conventional sub-region technique can be applied to model the multiple domains. By providing auxiliary conditions on interfaces, one may solve a system of simultaneous equations to obtain all boundary unknowns on the interfaces between the half-plane matrix and the inclusions. From the principle of superposition, loading on the half-plane surface can also be specified at the same time.

As a secondary step, the analysis of displacements/stresses at internal points in the half-plane is sometimes required when all boundary unknowns on the hole surfaces are determined by solving Eq. (1) via the standard collocation process. For the displacement analysis of internal points, the BIE in Eq. (1) is used with the source point P located at the internal point of interest and the free term C_{ij} set to be unity, that is

$$u_j(P) = \int_S U_{ij}^*\Big|_{\infty/2}(P,Q)t_i(Q)\,dS - \int_S T_{ij}^*\Big|_{\infty/2}(P,Q)u_i(Q)dS. \tag{21}$$

Here, it needs to be emphasized that the field point Q moves along the integration path of the holes in the clockwise direction such that the outward normal is always directed toward the centers of the holes.

For calculations of internal stresses, one needs to first compute the strains by the following BIE:

$$\varepsilon_{jl}(P) = \int_S U_{ijl}^*\Big|_{\infty/2}(P,Q)t_i(Q)\,dS - \int_S T_{ijl}^*\Big|_{\infty/2}(P,Q)u_i(Q)dS, \tag{22}$$

where

$$U^*_{ijl}\Big|_{\infty/2} = \frac{1}{2}\left(\frac{\partial\, U^*_{ij}\Big|_{\infty/2}}{\partial x^p_l} + \frac{\partial\, U^*_{il}\Big|_{\infty/2}}{\partial x^p_j}\right), \tag{23}$$

$$T^*_{ijl}\Big|_{\infty/2} = \frac{1}{2}\left(\frac{\partial\, T^*_{ij}\Big|_{\infty/2}}{\partial x^p_l} + \frac{\partial\, T^*_{il}\Big|_{\infty/2}}{\partial x^p_j}\right) \tag{24}$$

By performing the partial differentiations in Eqs. (23) and (24), one obtains

$$U^*_{ijl}\Big|_{\infty/2} = U^*_{ijl}\Big|_{\infty} + \frac{1}{R_\infty}\mathbf{Re}\left\{\sum_{m=1}^{2}\sum_{n=1}^{2} B_{im}D_{mn}\frac{\overline{\hat{G}'_{jln}}}{\hat{z}_{mn}}\right\}, \tag{25}$$

$$T^*_{ijl}\Big|_{\infty/2} = T^*_{ijl}\Big|_{\infty} - \frac{1}{R_\infty}\mathbf{Re}\left\{\sum_{m=1}^{2}\sum_{n=1}^{2} \hat{\mu}_{im}\frac{(n_1\mu_m - n_2)\, D_{mn}\overline{\hat{G}'_{jln}}}{\hat{z}^2_{mn}}\right\}, \tag{26}$$

where

$$\hat{G}'_{jln} = A_{jn}\hat{\mu}'_{ln} + A_{ln}\hat{\mu}'_{jn}, \tag{27}$$

and the $\hat{\mu}'_{kn}$ is defined by

$$\hat{\mu}'_{kn} = \begin{pmatrix} 1 & 1 \\ \mu_1 & \mu_2 \end{pmatrix}. \tag{28}$$

Eqs. (25) and (26), $U^*_{ijl}\Big|_{\infty}$ and $T^*_{ijl}\Big|_{\infty}$ are defined by

$$U^*_{ijl}\Big|_{\infty} = \frac{1}{R_\infty}\mathbf{Re}\left\{\sum_{k=1}^{2} B_{ik}\frac{\hat{G}_{jlk}}{z_k - z'_k}\right\}, \tag{29}$$

$$T^*_{ijl}\Big|_{\infty} = \frac{1}{R_\infty}\mathbf{Re}\left\{\sum_{k=1}^{2} \hat{\mu}_{ik}\frac{n_1\mu_k - n_2}{(z_k - z'_k)^2}\hat{G}_{jlk}\right\}. \tag{30}$$

After the strains at the internal point are obtained by Eq. (23), the corresponding stresses can be calculated using the generalized Hooke's law for anisotropy in a straight forward manner.

4 Numerical Examples

All formulations presented in this article have been implemented in an existing BEM code, using quadratic isoparametric elements. To illustrate the veracity as well as applicability in analyzing practical problems, three examples are investigated by the implemented code and verified by alternative approaches using either ANSYS or the BEM analysis for a very large domain. For practical applications, all analyses are for the state of plane strain.

Example I

For providing comparative analyses for problems of half-plane to be considered later, the first example (Example I) treats an infinitely large domain containing a semi-circular hole with radius R = 0.5(m) at the center as shown in Fig. 2. Two models can be used to simulate this problem, namely

Model I- using the Green's functions in Eqs. (10) and (11) for treating infinitely large domains and Model II- using a finite enclosed domain with dimensions comparably much larger than the hole size. Quartz is taken to be the material, that has the following principal properties (using conventional notations),

$$E_{11} = 34.5\ \text{GPa}, E_{22} = 51.6\ \text{GPa}, E_{33} = 25\ \text{GPa}, G_{12} = 3.7\ \text{GPa},$$
$$G_{23} = 54\ \text{GPa}, G_{31} = 6.3\ \text{GPa}, \nu_{12} = 0.28, \nu_{13} = 0.34, \nu_{23} = 0.28, \tag{31}$$
$$\mu_{31,23} = 0.4, \eta_{12,1} = \eta_{12,2} = \eta_{12,3} = 0.$$

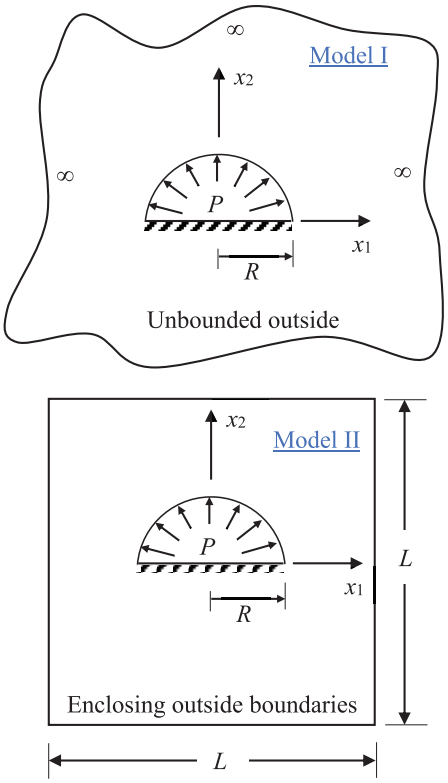

Figure 2: Models of a large domain containing a hole-Example I

To generate generally anisotropic properties, the principal axes are rotated 45° counterclockwise. In Model II, the side length $L = 10^4\ R$ was treated to simulate the infinitely large domain. For the BEM modeling of Model I, only 28 elements with 56 nodes were applied (Fig. 3); for Model II, double the number of elements were applied.

When the other one, i.e., Model I, cannot be simulated by the FEM, Model II was also simulated using ANSYS to provide comparative results, where 3080 PLANE182 elements with 9352 nodes were employed. Fig. 4 shows the modeling meshes of Model II by ANSYS. The hoop stresses on the upper surface of the hole were calculated to make the plots in Fig. 5.

As expected, peak values of the hoop stresses occur at $\theta = 45°$ and 135° except for the rapid rise-ups at $\theta = 0°$ and 180°, which are derived from the stress concentration at corners. In general, very ideal agreements between both analyses are present. From the comparison, it is apparent that both BEM analyses for either model, Model I for an infinite domain or Model II for a finite domain, are valid and

reliable. In addition, the internal stresses at a few sample points along $r = 0.55$ m were also calculated using Eq. (23) for Model I, where the Green's functions $U^*_{ijl}\big|_\infty$ and $T^*_{ijl}\big|_\infty$ were used as substitutes. The total displacements Δr and stresses are plotted in Figs. 6 and 7, respectively.

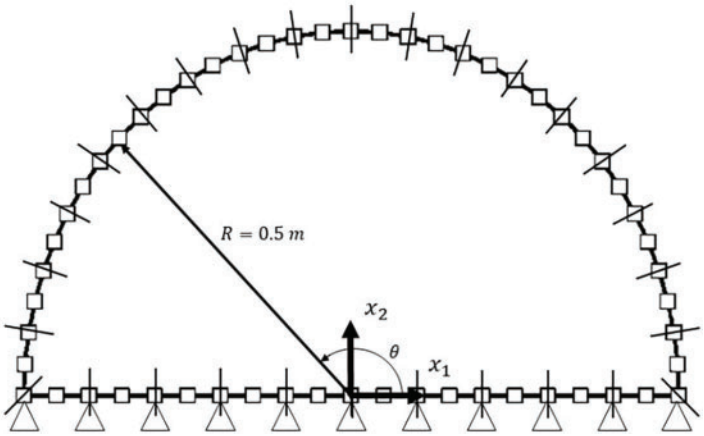

Figure 3: BEM modeling of Model I-Example I

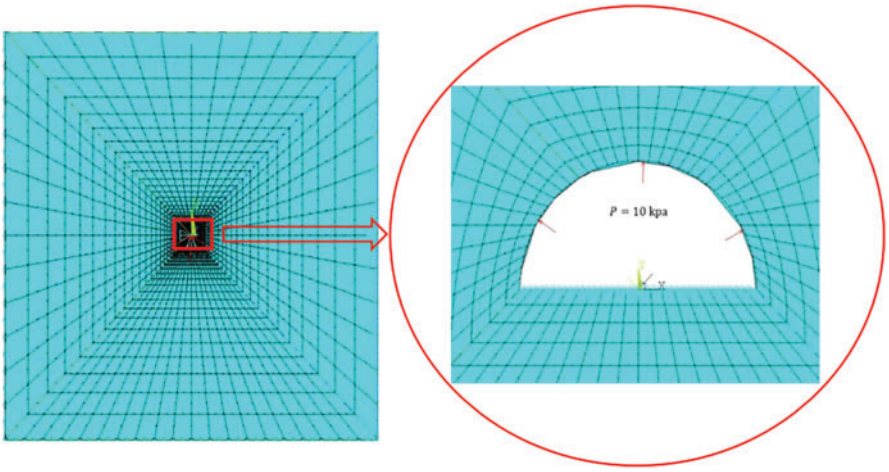

Figure 4: Modeling of Model II by ANSYS-Example I

Example II

The second example (Example II) considers a doubly adjoined container buried underground 5 m deep in a half-plane mining of quartz (Material 3) as shown in Fig. 8. Inside the enclosure is a semi-circular chamber, being subjected to uniform pressure $P = 100$ KPa. The flat surface of the container is completely constrained. The principal axes of the quartz are rotated 30° counterclockwise. Continuants of the composite container include (isotropic) concrete as Material 1 and (anisotropic) Glass/Epoxy as Material 2, where the following material properties were used,

$E = 24.5$ GPa, $\nu = 0.17$ for concrete,

$$E_{11} = 55.0 \text{ GPa}, E_{22} = 21.0 \text{ GPa}, E_{33} = 16.0 \text{ GPa}, \tag{32}$$

$G_{12} = 9.7$ GPa, $G_{23} = 62.0$ GPa, $G_{31} = 8.5$ GPa, for Glass/Epoxy,

$\nu_{12} = 0.25, \nu_{13} = 0.27, \nu_{23} = 0.19, \mu_{31,23} = 1.2,$

$\eta_{12,1} = \eta_{12,2} = \eta_{12,3} = 0.$

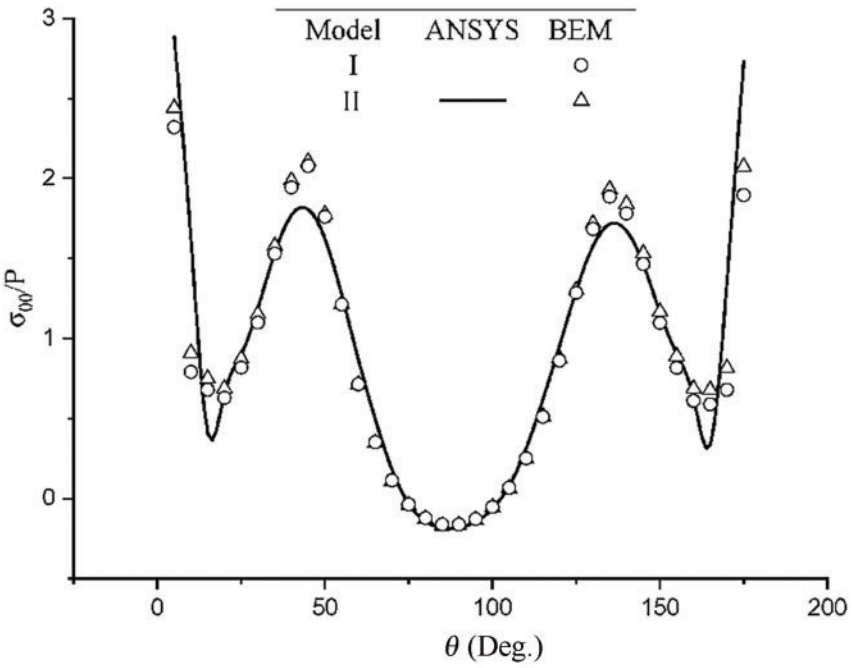

Figure 5: Distribution of the hoop stresses on the upper half of the hole-Example I

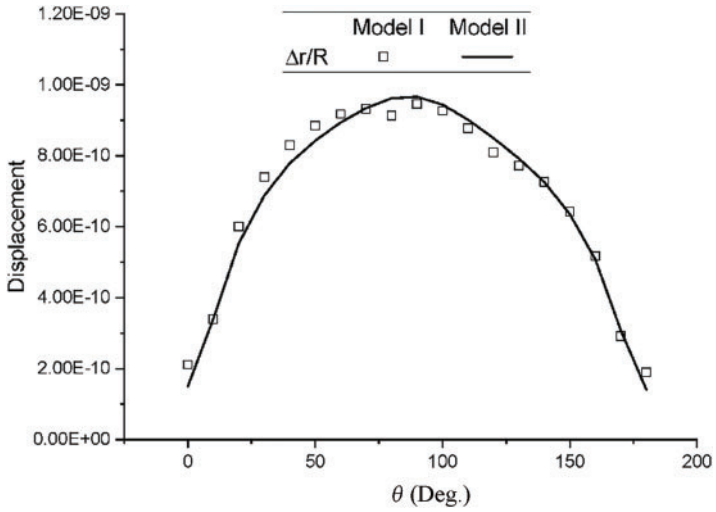

Figure 6: Distribution of the displacements on the upper half of the hole-Example I

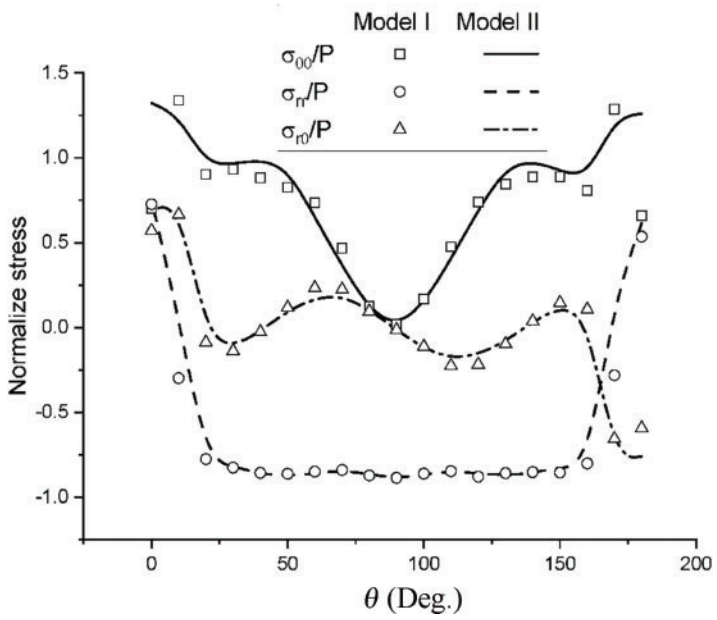

Figure 7: Stress components calculated at internal points $R = 0.55$ m-Example I

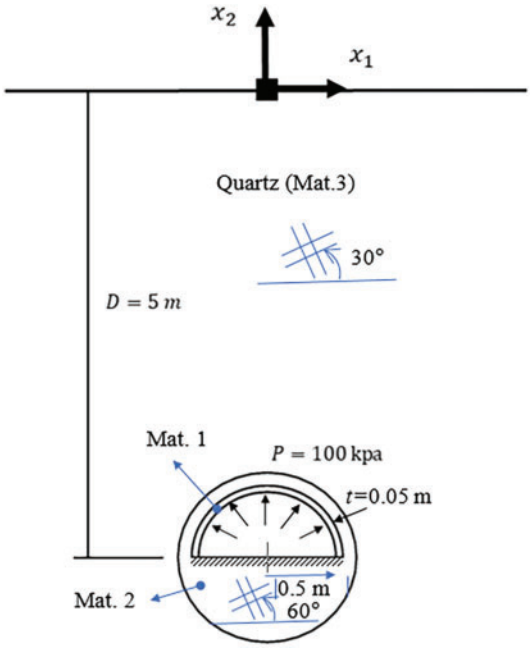

Figure 8: A doubly adjoined container buried underground-Example II

For yielding generally anisotropic properties, the principal axes of the Glass/Epoxy are rotated 60° counterclockwise. Fig. 9 shows the BEM meshes for the half-plane problem, i.e., by Model I, where 108 elements with 216 nodes were used. For providing comparative results, Model II with a very large rectangular enclosing boundary outside is simulated by the BEM, employing 124 elements with a total of 248 nodes.

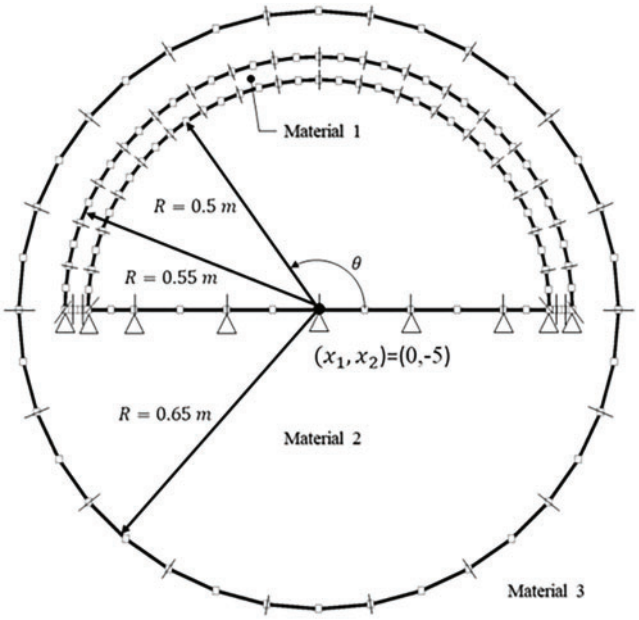

Figure 9: BEM meshes for the half-plane problem-Example II

It must be emphasized here that since the BEM analysis with a large finite domain has been verified for its validity in Example I, such analysis is trusted to be a comparative approach. Otherwise, the corresponding FEM analysis of this example will require intricate meshing to acquire convergently accurate results for comparison. Shown in Figs. 10 and 11 are the distributions of the radial stresses and hoop stresses on the surfaces of the upper-half enclosure.

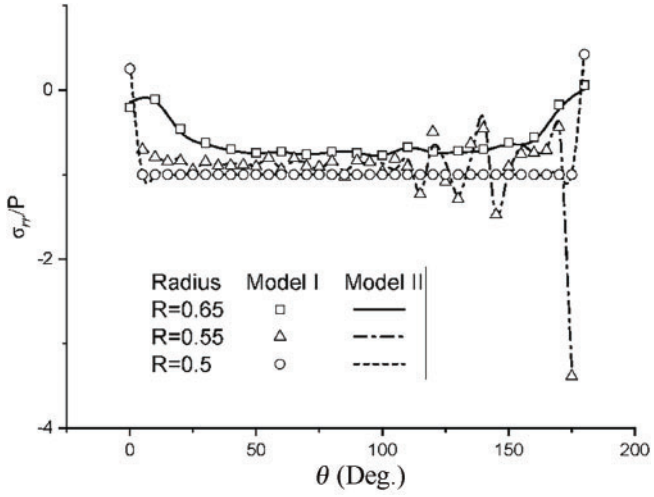

Figure 10: Radial stresses on the surfaces-Example II

In addition, all stress components at internal points along $r = 0.7$ m were calculated and plotted in Fig. 12. As can be seen from these comparisons from Figs. 10–12. The results calculated using Model I are indeed in agreement with those by Model II.

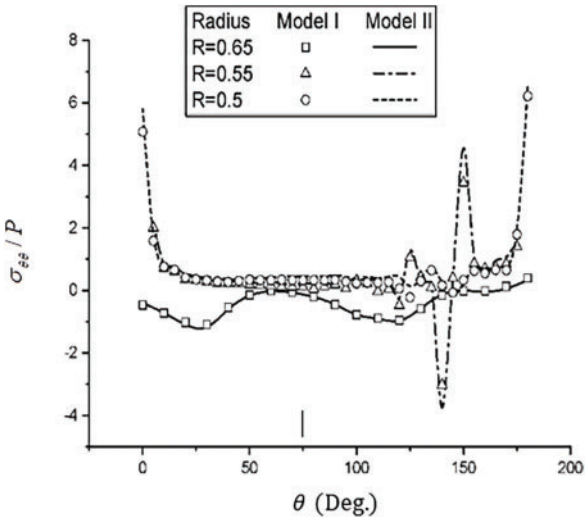

Figure 11: Hoop stresses on the surfaces-Example II

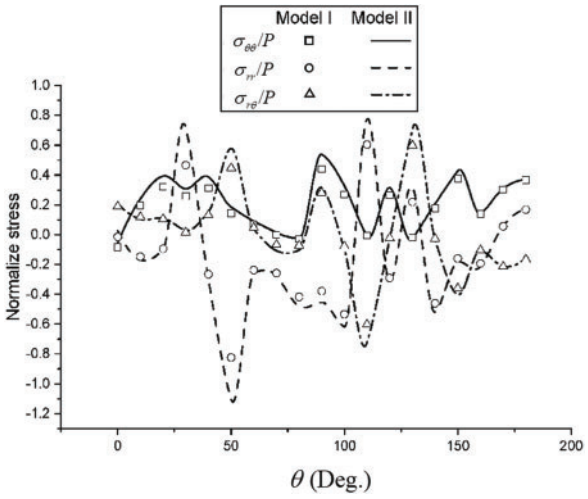

Figure 12: Stresses at internal points along $r = 0.77$ m-Example II

Example III

As the last example, Example III investigates a semi-circular hole with a radius $R = 0.5$ m in a bedrock mining of quartz as schematically shown in Fig. 13. For the boundary condition, the flat surface of the hole is fully constrained and uniform pressure spanning with width W is applied on the top surface of the half-plane with a distance D from the ground of the hole. This example is to analyze how the underground depth and the width of the applied load may affect the hoop stresses on the top surface of the hole. BEM meshing of Model I is also shown in Fig. 13, where only 28 elements with a total of 57 nodes were applied. To apply Model II for the analysis, an outside enclosing boundary with 5×10^5 m in width (x_1-axis) and 10^6 m in depth (x_2-axis) is added to give a total of 44 elements with 88 nodes applied. The principal axes of quartz are also rotated by 30° counterclockwise as in Example II. Distributions of hoop stresses along the circumferential surface of the upper hole calculated using both models are plotted in Fig. 14 for the case when $W = 1$ m. Shown in Fig. 15

are plots of the hoop stresses varied for different depths of the hole. As can be told from a mechanical sense, the hoop stresses decline with an increase of depth in the central region near 45°∼120°, while the trend goes reversely outside this central region. Fig. 16 plots the variation of hoop stresses for different loading widths. Also, it is interesting to see a similar trend present in Fig. 15. That is, larger hoop stresses for wider loading regions are only present in the central region but the trend goes reversely outside the region. In all cases, the results calculated using both models, Model I for a half-plane and Model II for a very large finite domain, agree with each other with negligible discrepancies observed only near corners.

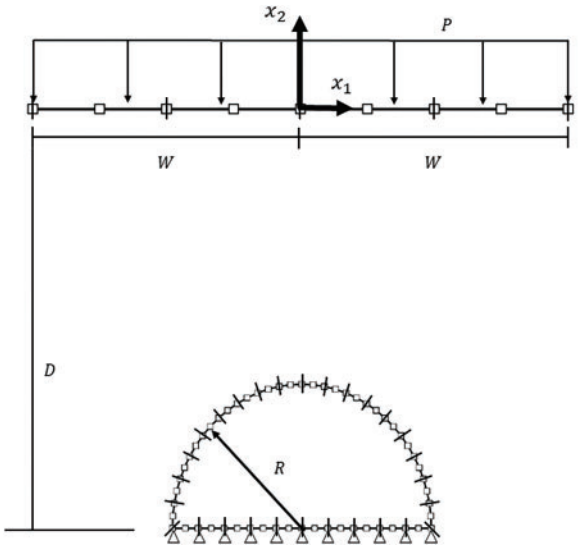

Figure 13: A semi-circular hole in the half-plane with loading on top-Example III

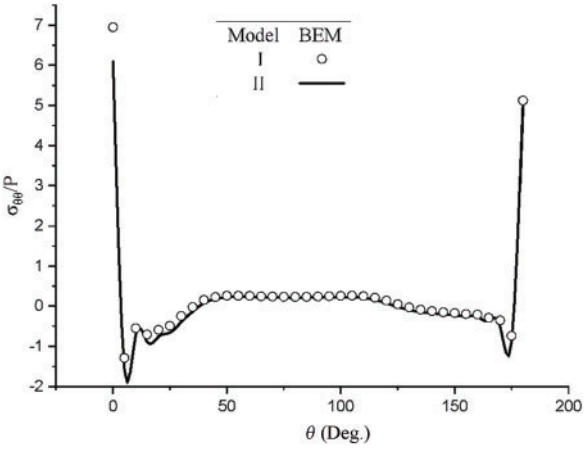

Figure 14: Distributions of hoop stresses on the hole surface-Example III

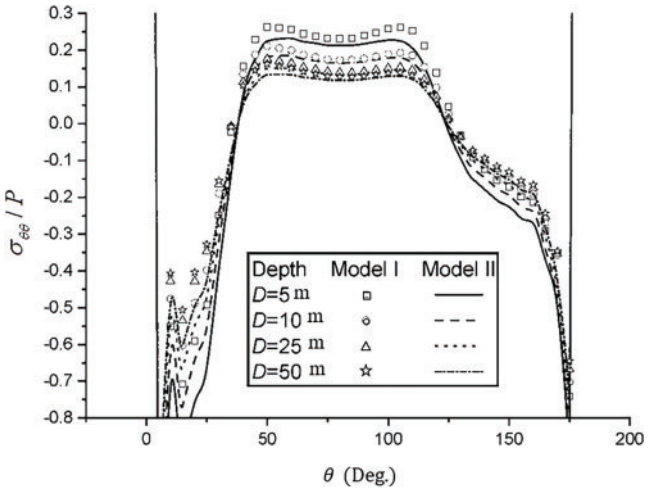

Figure 15: Hoop stresses on the hole surface for various depths-Example III

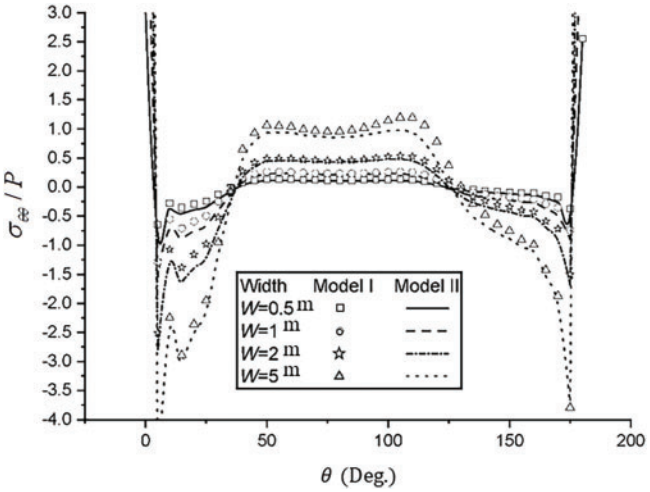

Figure 16: Hoop stresses on the hole surface for various loading width-Example III

5 Conclusions

In various disciplines of engineering, stress analysis of holes/inclusions in a half-plane has attracted significant research over the years. Despite mathematical elegance, analytical approaches cannot provide versatile analysis for complicated geometries and boundary conditions. For the elastic analysis of holes/inclusions in an anisotropic half-plane, this paper implements the fundamental solutions to treat problems of anisotropic half-plane, expressed as Lekhnitskii-like formulations. The fundamental solutions are further modified to vanish at infinity such that no meshes at infinity are required. In addition, the corresponding Somigliana's identity for calculating internal strains inside the anisotropic half-plane is also presented. Successful implementation of all presented formulations is demonstrated by studying a few example cases in the end. By comparing with the alternative BEM analysis employing a very large outside boundary to model infinity, the present half-plane analyses appear to be not only accurate but also very efficient, especially in the modeling itself. Conclusively,

the proposed BEM modeling of half-plane problems is very ideal to be applied to deal with various problems in engineering when the meshing of infinite boundaries is not involved in the modeling.

Acknowledgement: The graphical work by Liu, Tsung-Lun is acknowledged.

Funding Statement: This research was funded by the National Science and Technology Council, Taiwan, grant number: 113-2221-E-006-122.

Author Contributions: The authors confirm contribution to the paper as follows: study conception and design: Yui-Chuin Shiah; data collection: Chao-Chun Ko; analysis and interpretation of results: Chao-Chun Ko; draft manuscript preparation: Yui-Chuin Shiah. All authors reviewed the results and approved the final version of the manuscript.

Availability of Data and Materials: The data that support the findings of this study are available from the corresponding author, YCS, upon reasonable request.

Ethics Approval: Not applicable.

Conflicts of Interest: The authors declare no conflicts of interest to report regarding the present study.

References

1. Ru CQ. Analytical solution for Esheby's problem of an inclusion of arbitrary shape in a plane or half-plane. J Appl Mech. 1999;66(2):315–22. doi:10.1115/1.2791051.
2. Pan E. Eshelby problem of polygonal inclusions in anisotropic piezoelectric full- and half-planes. J Mech Phys Solids. 2004;52(3):567–89. doi:10.1016/S0022-5096(03)00120-0.
3. Mogilevskaya SG. The complex one-sided integrals of Cauchy and Hadamard and application to boundary element method. Int J Numer Anal Meth Geomech. 1998;22(12):947–68. doi:10.1002/(ISSN)1096-9853.
4. Sudret B. Multiphase model for inclusion-reinforced geostructuresapplication to rock-bolted tunnels and piled raft foundations. Int J Numer Anal Meth Geomech. 2001;25(2):155–82. doi:10.1002/nag.123.
5. Muskhelishvili NI. Some basic problems of mathematics theory of elasticity. Groningen: Noordhorff; 1953.
6. Eshelby JG. The determination of the elastic field of an ellipsoidal inclusion, and related problems. Proc R Soc Lond. 1957;241:376–96.
7. Jammes M, Mogilevskay SG, Crouch SL. Multiple circular nano-inhomogeneities and/or nano-pores in one of two joined isotropic elastic half-planes. Eng Anal Bound Elem. 2009;3(2):233–48. doi:10.1016/j.enganabound.2008.03.010.
8. He LH, Li ZR. Impact of surface stress on stress concentration. Int J Solids Struct. 2006;43(20):6208–19. doi:10.1016/j.ijsolstr.2005.05.041.
9. Zienkiewicz OC, Cheung YK, Stagg KG. Stresses in anisotropic media with particular reference to problems of rock mechanics. J Strain Anal. 1966;1:172–82. doi:10.1243/03093247V012172.
10. Barla G. Stresses around a single underground opening near a tension-free surface. Int J Rock Mech Min Sci Geomech Abstr. 1972;9:103–26.
11. Soliman E, Duddeck H, Ahrens H. Two- and three dimensional analysis of closely spaced double-tube tunnels. Tunell Undergound Space Technol. 1993;8:13–18.
12. Atluri SN, Zhu T. New concepts in meshless method. Int J Numer Meth Eng. 2000;47:537–56. doi:10.1002/(ISSN)1097-0207.

13. Aggarwal R, Lamichhane BP, Meylan MH, Wensrich CM. An investigation of radial basis function method for strain reconstruction by energy-resolved neutron imaging. Appl Sci. 2021;11(1):391. doi:10.3390/app11010391.
14. Dong CY, Lo SH, Cheung YK. Numerical solution for elastic inclusion problems by domain integral equation with integration by means of radial basis functions. Engng Anal Bound Elem. 2004;28:623–32.
15. Dong CY, Lee KY. Stress analysis of an infinite anisotropic elastic medium containing inclusions using the boundary point method. Engng Anal Bound Elem. 2004;28:1293–302.
16. Telles JCF, Brebbia CA. Boundary element solution for half-plane problems. Int J Solids Struct. 1981;17:1149–58.
17. Meek JL, Dai C. Boundary element modeling: near surface excavations. Comput Meth Appl Mech Eng. 1993;102:15–27.
18. Dong CY, Lo SH. Boundary element analysis of an elastic half-plane containing nanoinhomogeneities. Comput Mater Sci. 2013;73:33–40. doi:10.1016/j.commatsci.2013.02.014.
19. Mogilevskaya SG, Crouch SL, Stolarski HK. Multiple interacting circular nano-inhomogeneities with surface/interface effects. J Mech Phys Solids. 2008;56(6):2298–327. doi:10.1016/j.jmps.2008.01.001.
20. Dumir PC, Mehta AK. Boundary element solution for elastic orthotropic half-plane problems. Comput Struct. 1987;26(3):431–8. doi:10.1016/0045-7949(87)90043-5.
21. Lekhnitskii SG. Theory of elasticity of an anisotropic bod. San Francisco, CA, USA: Holden Day; 1963.
22. Tan CL, Gao YL, Afagh FF. Anisotropic stress analysis of inclusion problems using the boundary integral equation method. J Strain Anal. 1992;7(2):67–76. doi:10.1243/03093247V272067.
23. Suo Z. Singularities, interfaces and cracks in dissimilar anisotropic media. Proc R Soc Lond. 1990;A427:331– 58.
24. Pan E, Chen CS, Amadei B. A BEM formulation for anisotropic half-plane problems. Eng Anal Bound Elem. 1997;20(3):185–95. doi:10.1016/S0955-7997(97)00081-7.
25. Beskou ND. Dynamic analysis of an elastic plate on a cross-anisotropic and continuously nonhomogeneous viscoelastic half-plane under a moving load. Acta Mech. 2020;231(4):1567–85. doi:10.1007/s00707-019-02594-6.
26. Nguyen VT, Hwu C. Indentation by multiple rigid punches on two-dimensional anisotropic elastic or viscoelastic solids. Int J Mech Sci. 2020;178(9):105595. doi:10.1016/j.ijmecsci.2020.105595.
27. Hasebe N. Stress analysis for an orthotropic elastic half plane with an oblique edge crack and stress intensity factors. Acta Mech. 2021;232(3):967–82. doi:10.1007/s00707-020-02894-2.
28. Csáki E, Földes A. On the local time of the half-plane half-comb walk. J Theor Probab. 2022;35(2):1247–61. doi:10.1007/s10959-020-01065-2.
29. Nguyen VT, Hwu C. A unified full field solution for indentation of an anisotropic piezoelectric half-plane by multiple rigid punches. Mech Adv Mater Struct. 2023;30(19):3897–911. doi:10.1080/15376494.2022.2084802.
30. Nguyen VT, Chen G-T, Hwu C. Multibody contact of two-dimensional anisotropic elastic/piezoelectric/magneto-electro-elastic solids. Eng Anal Bound Elem. 2023;146(26):767–85. doi:10.1016/j.enganabound.2022.11.019.
31. Li M, Wang Y-L. Zero-viscosity limit for Boussinesq equations with vertical viscosity and Navier boundary in the half plane. Nonlinear Anal Real World Appl. 2024;80:104150.
32. Dinh N, Duc N, Thuong V. Surface green's functions for an anisotropic viscoelastic half-plane and their application to contact problems. Eng Anal Bound Elem. 2024;167(4):105884.doi:10.1016/j.enganabound.2024.105884.
33. Hwu C. Anisotropic elastic plates. Springer Science+Business Media, LLC, 233 Spring Street, New York, NY, USA: Springer-Verlag US; 2010 [cited 2024 Dec 22]. Available from: https://link.springer.com/book/10.1007/978-1-4419-5915-7.